GEOPHYSICS, VOL. 72, NO. 2 (MARCH-APRIL 2007); P. G1–G8, 8 FIGS.
10.1190/1.2424542

Seismoelectric data processing for surface surveys of shallow targets

Seth S. Haines[1], Antoine Guitton[2], and Biondo Biondi[3]

ABSTRACT

The utility of the seismoelectric method relies on the development of methods to extract the signal of interest from background and source-generated coherent noise that may be several orders-of-magnitude stronger. We compare data processing approaches to develop a sequence of preprocessing and signal/noise separation and to quantify the noise level from which we can extract signal events. Our preferred sequence begins with the removal of power line harmonic noise and the use of frequency filters to minimize random and source-generated noise. Mapping to the linear Radon domain with an inverse process incorporating a sparseness constraint provides good separation of signal from noise, though it is ineffective on noise that shows the same dip as the signal. Similarly, the seismoelectric signal and noise do not separate cleanly in the Fourier domain, so *f-k* filtering can not remove all of the source-generated noise and it also disrupts signal amplitude patterns. We find that prediction-error filters provide the most effective method to separate signal and noise, while also preserving amplitude information, assuming that adequate pattern models can be determined for the signal and noise. These Radon-domain and prediction-error-filter methods successfully separate signal from >33 dB stronger noise in our test data.

INTRODUCTION

Development of data processing techniques is one of the most important steps toward regular use of the seismoelectric method in near-surface (and exploration) geophysics. Effective data processing techniques with known efficacy will lead to better (more realistic) target selection and improved survey design and it also will facilitate accurate interpretation of the resulting data.

The coseismic field is the electric field induced by, and located within, a propagating compressional seismic wave, that is created by pressure gradient-induced electrokinetic effects (e.g., Pride and Haartsen, 1996; Garambois and Dietrich, 2001; Haines, 2004). In seismoelectric data, the coseismic field appears as coherent arrivals corresponding with the passage of the seismic waves through the electrode array and shows virtually the same waveform and moveout as the seismic body wave (Garambois and Dietrich, 2001). The interface response is the electromagnetic disturbance that occurs when a compressional wave encounters an interface in mechanical, electrical, or chemical properties. Because the coseismic field often obscures the interface response (and can be several orders-of-magnitude stronger, cf. Butler et al., 2002), we consider the coseismic field to be noise.

The electric potential of the interface response Φ (measured at a horizontal offset x and depth z) can be approximated (e.g., Thompson and Gist, 1993; Garambois and Dietrich, 2001) as that of an electric dipole (e.g., Landau and Lifshitz, 1984):

$$\Phi(x,z) = \frac{I}{2\pi\sigma}\frac{z}{(x^2 + z^2)^{3/2}}, \tag{1}$$

where I is the magnitude of the electric current excited by the seismic wave, and σ is the electrical conductivity of the soil. The interface response is created at the first Fresnel zone directly beneath the shotpoint (for a horizontal subsurface interface). In contrast to seismic reflection, only one interface response event occurs, at one subsurface location per interface, for a given seismic source location. It is measured approximately simultaneously at all receiver locations; that is, it shows no moveout relative to the coseismic arrivals (electromagnetic velocity V_{EM} is much greater than the seismic P wave velocity V_P). Garambois and Dietrich (2002) provide a thorough discussion of the location and size of the seismoelectric Fresnel zone. The interface response electric field is essentially that of a dipole, so measured potential differences show opposite polarity on opposite sides of the shotpoint and have a distinct pattern (equation 1) that can

Manuscript received by the Editor December 7, 2004; revised manuscript received September 21, 2006; published online January 30, 2007.
[1]Formerly Stanford University, Department of Geophysics, Stanford, California; presently U.S. Geological Survey, Denver, Colorado. E-mail: shaines@usgs.gov.
[2]Formerly Stanford University, Department of Geophysics, Stanford, California; presently 3DGeo Development Incorporated, Santa Clara, California. E-mail: antoine@3dgeo.com.
[3]Stanford University, Department of Geophysics, Stanford, California. E-mail: biondo@sep.stanford.edu.

be used to discriminate the interface response from other recorded arrivals. Though the direct field (Haines et al., 2004; Haines, 2004) shows the same amplitude pattern, it occurs only at the source point and generally exists for less than 20 ms so is not problematic for surface surveys targeting layers deeper than a few meters (assuming a seismic velocity corresponding with unsaturated sediments) or for any survey in which the source and receivers are separated by sufficient distance.

The sinusoidal subtraction and frequency revision methods presented by Butler and Russell (1993, 2003) effectively remove power line noise from seismoelectric records, and represent a key first step in seismoelectric data processing. Wiener filters (Thompson and Gist, 1993), radial trace transforms (Butler et al., 2002), and *f-k* filtering of virtual shot gathers (Kepic and Rosid, 2004) have been tested as seismoelectric signal/noise separation approaches, but none of these methods has proven to be adequately effective.

An effective seismoelectric data processing sequence must remove background and coseismic fields from a seismoelectric shot gather such that it can be stacked to produce a trace dominated by interface response arrivals, for use in a seismoelectric image. Our objective is to develop such a sequence and to quantitatively assess its performance so that we understand the sensitivity possible with this processing approach. We begin by discussing preprocessing techniques and then compare signal/noise separation methods using test shot gathers that contain synthetic interface response events and field-collected or numerically modeled noise, building on the work of Haines et al. (2003). We test *f-k* filtering and linear Radon transforms (e.g., Yilmaz, 2001), both of which attempt to separate the interface response from coseismic fields based on dip. We also compare results using a pattern-based approach employing prediction-error filters (PEFs) (Claerbout and Fomel, 2001; Guitton, 2005) that exploits the interface response amplitude pattern as well as its dip. We then present our preferred processing flow and discuss necessary further advances in seismoelectric data processing.

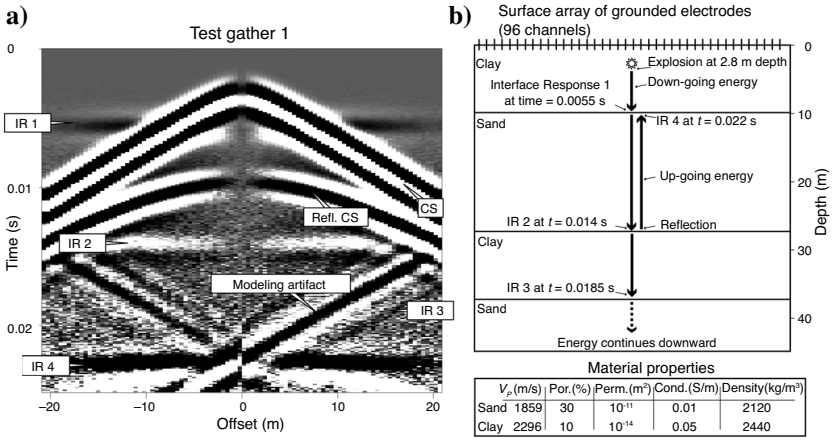

Figure 1. (a) Test gather 1: synthetic seismoelectric data. Arrows and labels identify the seismoelectric arrivals. It is our goal to remove the curved and dipping energy, and to enhance the flat interface response events including the hidden IR 3. Data are scaled by t^2, and the polarity of the negative-offset traces is reversed, for comparison with later figures. (b) The geologic model used for calculation of synthetic data shown in part (a). Thick arrows indicate raypaths for seismic energy that creates seismoelectric interface response events. In addition to the down-going energy that creates interface response events IR 1, IR 2, and IR 3, up-going (reflected) seismic energy creates IR 4. In addition, the direct and reflected seismic arrivals are recorded as coseismic noise (the curved arrivals). Material properties are shown in the table (P-wave velocity, porosity, hydraulic permeability, electrical conductivity, and bulk density).

TEST DATA

Test gather 1: Synthetic seismoelectric data

Synthetic data facilitate the evaluation of processing techniques while avoiding the complexities and expenses of field data. The 96-channel shot gather shown in Figure 1a was created using the finite-difference modeling approach described by Haines and Pride (2006). It corresponds with the geologic model shown in Figure 1b, consisting of alternating unconsolidated clay and sand layers whose material properties are shown in the figure. All layers are saturated with pore water of pH 7 and salinity 0.001 mol/L. Zeta potential is calculated using the relations provided by Pride and Morgan (1991). We model an explosive source (2.8-m depth, 400-Hz Ricker wavelet) that provides the energy that is then recorded by 96 pairs of electrodes at the surface of the model. The width of each dipole pair is 1.4 m, and the spacing between the centers of the pairs is 0.44 m. Uniform white noise has been added to the gather for realism [rms ratio of the synthetic data (all events) to added white noise is 60:1, which is more than twice as much background noise as we observe at our field sites]. The plotted data are scaled by t^2 for comparison with results in later figures.

Within the gather are four interface response events that we wish to separate from the curved coseismic energy, the dipping modeling artifacts, and the random noise; all are identified in Figure 1a. The first interface response event (IR 1) was created when the down-going P-wave encountered the first interface. IR 2 corresponds with the second interface, and the unseen IR 3 corresponds with the third interface. The amplitude of event IR 3 is below the level of the added random noise. The interface response event labeled IR 4 was created when the reflected P-wave traveling upward from the second interface encountered the first interface. It has a higher amplitude than IR 3 because the interface is much shallower, but lower amplitude than IR 1, because only a fraction of the seismic energy is reflected upward at the interface and because of energy loss associated with the longer distance traveled (divergence only; this modeling does not include absorption other than the negligible loss due to Biot flow).

The data contain the coseismic fields of the seismic wave reflected from the first interface (labeled Refl. CS in Figure 1a) and the seismic direct wave (CS, arriving after time zero and appearing curved because the shot is at a depth of 2.8 m below the electrodes). The data also contain dipping modeling artifacts that we consider to be additional noise to be removed from the data. The data do not include Rayleigh waves because our modeling code does not include a free surface. Because of this limitation, and the other nonrealistic aspects of test gather 1, we also test our processing techniques on the more realistic shot gather described next.

Test gather 2: Field data plus synthetic signal events

Field data provide a more realistic assessment of data processing options than synthetic data, but uncertainties in seismoelectric data interpretation (this is a method that is in development) complicate assessment of results. With data processing

improvements will come greater certainty in interpretation of events revealed by data processing, but these developments can not occur simultaneously. In order to provide a certain, quantitative assessment of signal/noise separation techniques based on realistic data, we target synthetic events added to field data.

Test gather 2 is shown in Figure 2a, with dipping coseismic energy and flat direct field arrivals labeled ($t^{1.85}$ scaling has been applied for comparison with later figures). This gather is the result of stacking 25 impacts of a 5.4-kg sledgehammer on a hammer plate located ~0.5 m from the center of a 48-channel electrode array with 0.4 m spacing between electrode dipoles that are 1.4 m wide (the dipoles overlap). The array was deployed at a site with clay-rich soil to a depth of at least 3 m [the vineyard site that is described in more detail by Haines (2004) and Haines et al. (2007)]. The data were collected with a 24-bit Geometrics Geode seismograph that offers a nominal 110-dB instantaneous dynamic range which should be ample for the data that we record (the dynamic range of features of interest in our field data is < 50 dB). With the strong display gains used in Figure 2, flat (no moveout) noise is evident below 0.07 s at near-zero offsets and at offsets > ~5 m. The amplitude pattern is not that of a dipole that corresponds with these arrival times, so these arrivals must be interpreted as noise. Noise from a distant source would be expected to show the same polarity (and similar amplitude) on all recording channels. The near-zero-offset arrivals appear to be source-related (their true polarity is reversed on opposite sides of the shotpoint), and may be weak seismoelectric direct fields created by hammer bounce on the impact plate. The flat noise at offsets > ~5 m shows a different polarity-reversal location and is likely remnant power line noise associated with a water pipe that is buried near that edge of the field site.

To the field data we have added three synthetic interface response events, shown separately in Figure 2b. These events were created using a Ricker wavelet (dominant frequency 150 Hz) and the assumption [following Garambois and Dietrich (2001)] that the interface response from a particular depth z is equivalent to the summation of the fields of many electric dipoles (potential calculated using equation 1) distributed across the first Fresnel zone. We calculate the radius of the first Fresnel zone using the simple relation (e.g., Sheriff and Geldart, 1995) $r = \sqrt{\frac{\lambda}{2}\left(z + \frac{\lambda}{8}\right)}$, for a wavelength λ calculated using the dominant frequency of the wavelet and a constant velocity v = 400 m/s. We assume that the Fresnel zone is centered directly beneath the shotpoint, as for horizontal layers (Thompson and Gist, 1993). The hidden interface response events have signal-to-noise ratios of: IR A, −30 dB; IR B, −41 dB; IR C, −33 dB. These ratios were calculated using rms amplitudes determined for 0.006-s windows (spanning the three largest lobes of the added waveforms) of the field record and synthetic events prior to their summation.

The original field data do not contain any hidden interface response events that we can interpret with certainty. If the data do contain hidden events, we can conclude that they are below the signal-to-noise ratio of any added synthetic events that are revealed through data processing. Because the added events are realistic and have known amplitudes and arrival times, and because the noise is data collected in the field, this shot gather provides a valuable, quantitative, and realistic test of signal/noise separation methods. This approach is preferable to blindly processing data to reveal events of uncertain origin, though admittedly inferior to targetting definitively interpretable hidden events. It is hoped that future seismoelectric method development will make possible the confident interpretation of the interface response from layers at depth, and that our work with this partially synthetic shot gather represents progress toward that goal.

DATA PREPROCESSING

We consider seismoelectric data **d** to be the sum of background noise $\mathbf{n}_{bg}$, coseismic noise $\mathbf{n}_{cs}$, and interface response signal **s**: $\mathbf{d} = \mathbf{n}_{bg} + \mathbf{n}_{cs} + \mathbf{s}$. We employ preprocessing steps to minimize coseismic fields and to remove the background noise $\mathbf{n}_{bg}$, which includes harmonic noise from the power grid and any local sources (pumps, generators, etc.) along with noise spikes (from distant lightning strikes, etc).

The shot gather shown in Figure 3a was chosen for comparison of power line noise removal techniques because it contains particularly difficult-to-remove harmonic noise from the power grid (60 Hz and its harmonics). The seismic source in this case is 0.15 kg of explosive located 12 m perpendicularly away from the center of the receiver electrode array. Between the source and receivers were two vertical targets (sand-filled trenches), described in detail by Haines (2004). The electrode dipoles were 1.05-m wide, and spaced at 0.7 m. Application of the *sinusoidal subtraction* technique of Butler and Russell (1993) to the data in Figure 3a yields the result shown in Figure 3b. A significant amount of harmonic noise remains, making interpretation of flat events difficult. This remnant noise is at least partially due to deviation of the fundamental frequency from 60.00 Hz in traces adjacent to a water pipe that is buried near the end of the receiver array. The computationally more intensive *frequency revision* approach described by Butler and Russell (2003) yields the improved result shown in Figure 3c. We can now identify the interface response event (marked by the two arrows) created at the trench nearer to the receiver electrodes.

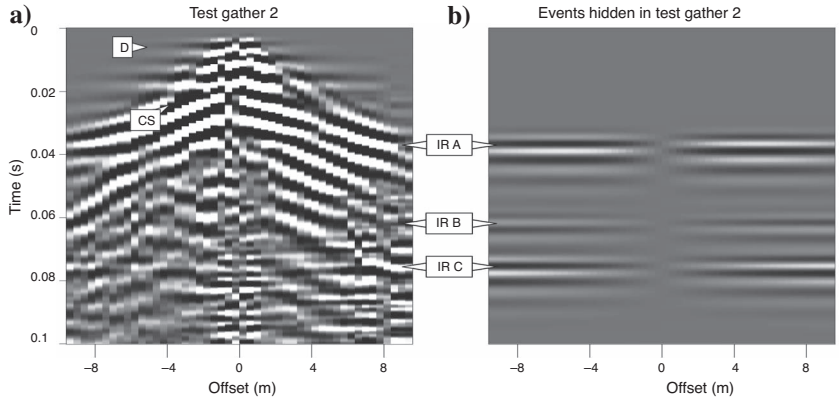

Figure 2. (a) Test gather 2: sledgehammer-source seismoelectric shot gather with three added synthetic interface response events. Harmonic noise from the power grid (60 Hz) has been removed from the field data using the methods described by Butler and Russell (1993). (b) Synthetic events that were added to field data to produce test gather 2. Display filter: 120–500 Hz; display gain: $t^{1.85}$. Polarity of negative-offset traces is reversed for comparison with later figures.

We find that unstacked shot records (such as the data in Figure 3) present the most challenging power line noise problem, and frequently require the computational expense of the frequency revision method. With sledgehammer stacking, minor deviations of the fundamental frequency in individual prestack shot gathers tend to be less problematic, and thus the sinusoidal subtraction technique is generally sufficient. For instance, the hammer-source data shown in Figure 2a have been processed with the sinusoidal subtraction technique; the frequency revision method technique yields negligible improvement for this shot gather. This trend is likely due to the tendency of the (uncorrelated) power line noise to stack out of sledgehammer records relative to the signal. Both of these methods are superior to notch filtering at 60 Hz and all of its harmonics up to the Nyquist frequency because they do not alter the frequency content of the seismoelectric data.

The signal-to-noise ratio between the interface response signal and the coseismic field can often be improved with low-cut filters. The frequency content of the interface response is the same as the frequency content of the seismic wave that interacts with the interface and produces the response. We record the interface response within the electromagnetic near-field (the region where the fields are diffusive rather than propagating) such that absorption of the electromagnetic energy is negligible. Thus for many recording geometries the interface response will be of higher frequency than the coseismic field (e.g., the interface response from a layer at depth will have higher frequency content than the coseismic field of the P-wave reflection from the same layer). In addition, the coseismic field associated with surface waves will tend to have lower frequency content than the interface response from a layer at depth (just as ground roll in a seismic record is generally of lower frequency than other seismic arrivals). Other frequency filtering can help to minimize background noise (e.g., removal of high-frequency spikes with high-cut filters).

As with seismic reflection processing, we boost the amplitude of low-amplitude interface response signals from deeper (or more distant) interfaces with standard procedures such as automatic gain control (AGC) or gains corresponding with multiplication of each sample in a trace by a scalar that is the arrival time raised to a certain power (e.g., t^2). In some cases it is beneficial to apply these gains before signal/noise separation (but after harmonic noise subtraction), to boost the amplitude of later arrivals so that they have equal importance in the residual of inversion schemes.

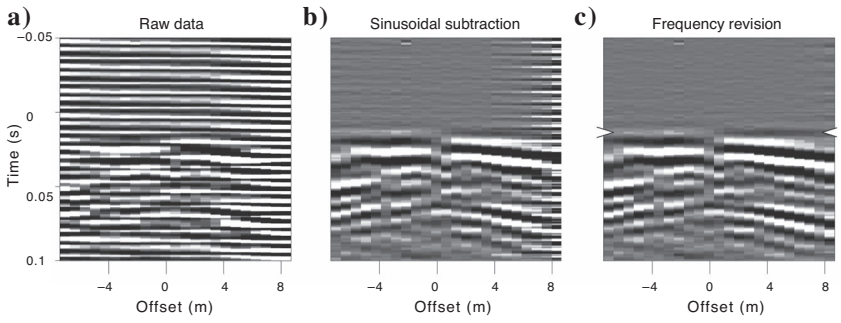

Figure 3. Power line noise removal comparison. All are plotted with 100 to 500 Hz bandpass filtering. Raw data (a) consist of a shot gather recorded with an explosive source located 12 m perpendicularly away from the center of the receiver line. The gather after sinusoidal subtraction (b) shows considerably less power line noise. After application of the frequency revision technique, the data (c) show the previously obscured interface response event that is marked by the two arrows.

INTERFACE RESPONSE/COSEISMIC FIELD SEPARATION METHODOLOGIES

Assuming that preprocessing has been successful, our data are now the sum of only interface response energy **s** and coseismic field energy $\mathbf{n}_{cs}$: $\mathbf{d} = \mathbf{n}_{cs} + \mathbf{s}$. It is our goal to separate these two forms of energy, and although coseismic noise may be of much greater magnitude, we can exploit three unique attributes of the interface response energy to identify and extract it from a record. The interface response has the amplitude pattern of a dipole (equation 1) and shows opposite polarity on opposite sides of the shotpoint. In addition, it shows virtually zero moveout because it travels (diffuses) at V_{EM} which is several orders-of-magnitude greater than the apparent velocity V_P of the coseismic field.

Frequency-wavenumber filtering

Muting in the frequency-wavenumber (f-k) domain (or Fourier domain) is a standard and commonly used technique for separating seismic arrivals based on dip (e.g., Yilmaz, 2001), and so is a logical choice for seismoelectric data. We apply mutes in the f-k domain that are symmetrical and fan shaped with sine-squared tapers. The consistency of test gather 1 permits a high mute velocity of 10^5 m/s, while the irregularities of test gather 2 force us to choose a moderate velocity cut-off of 8000 m/s. In addition, we eliminate the near-offset (less-than 4 m) traces for test gather 2 prior to f-k filtering to avoid poor separation of the flat signal from the flat parts of the near-offset coseismic noise.

Radon-domain filtering

Radon transforms (e.g., Yilmaz, 2001) map from the t-x domain to the τ-p domain (τ is the zero-offset intercept of an event of slowness p), based on summation along trajectories that are linear or curved. We find that the linear Radon transform (LRT) provides better separation of seismoelectric data in the τ-p domain than parabolic or hyperbolic transforms. We employ an iterative inversion process (Thorson and Claerbout, 1985) to determine, in a least-squares sense, the τ-p domain mapping **m** that best corresponds to the data **d**, as related by the Radon operator **L**. Thus we minimize the objective function

$$f(\mathbf{m}) = \|\mathbf{Lm} - \mathbf{d}\|^2. \tag{2}$$

We include a Cauchy regularization term (Sacchi and Ulrych, 1995) to enforce sparseness (improve focusing) in the model space (the Radon domain). This provides cleaner separation of signal from noise and helps minimize artifacts that would otherwise exist. Our objective function for a model space of size n may be written as (Sava and Guitton, 2005)

$$f(\mathbf{m}) = \left\|\mathbf{Lm} - \mathbf{d}\right\|^2 + \epsilon^2 b^2 \sum_{i=1}^{n} ln\left(1 + \frac{m_i^2}{b^2}\right), \tag{3}$$

where ϵ and b are constants, chosen a priori, that allow us to control the degree of sparseness in the model (ϵ) and the minimum value below which

energy in the Radon domain is zeroed (b). This objective function is nonlinear so we use the limited-memory quasi-Newton method described by Guitton and Symes (2003) to find the τ-p model that corresponds with the minimum value of $f(\mathbf{m})$.

Interface response signals map to the slowness axis of the τ-p domain ($p \approx 0$) while noise maps elsewhere ($|p| > 0$). We find that it is important to perform a polarity flip on the seismoelectric data before Radon transformation, so that interface response events have constant polarity and thus collapse smoothly to points in the Radon domain. We mute in the τ-p domain using narrow, tapered, rectangular mutes centered around the slowness axis. Data imperfections cause imperfect mapping in the τ-p domain which may leave some data energy in the model residual. To address this, we prefer to model the noise (by muting the signal from the τ-p domain), map it back to t-x space and then subtract it from the data. The Radon domain mapping of test gather 1 is shown in Figure 4a. We have applied a t^2 gain before Radon transformation so that weaker events later in the record are not inadvertently removed by the regularization. We then mute energy with slowness <0.00008 s/m (shown by the dark lines in Figure 4a), to create an estimated noise model. Test gather 2 (τ-p mapping shown in Figure 4b) was processed similarly, but with a $t^{1.85}$ gain applied before transformation, and mute lines set at 0.0006 s/m. The scaling powers were experimentally chosen to provide a smooth amplitude distribution in each gather. Sparseness, as enforced by the Cauchy regularization, is apparent in both plots and leads to a better signal/noise separation than without the sparseness constraint.

Prediction-error filters

We can take advantage of both the amplitude and pattern characteristics of our signal/noise separation problem by implementing a technique using PEFs (Claerbout and Fomel, 2001) **S** and **N** to estimate the signal and noise, respectively. Following Guitton (2005), we use pattern models to obtain **S** and **N** and then use these nonstationary PEFs to separate the signal and noise in a least-squares inversion. A key requirement for clean separation is the availability of suitable pattern models for PEF estimation (models that closely resemble the signal and noise) to produce PEFs that accurately convey the essential aspects of the signal and noise. The dimensions of PEFs **S** and **N** are largely determined through experimentation, though experience and common sense suggest that the flat interface response energy can best be modeled by PEFs that extend farther in the offset direction than in the time direction. The coseismic noise, since its dimensions are more equal in offset and time, is often best modeled by PEFs that have a similar number of elements in the time and offset directions (or perhaps a slightly greater number of elements in the time direction to correspond with fast time-sample rates).

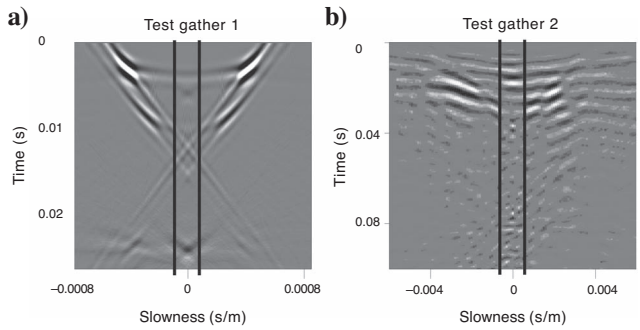

Figure 4. Linear Radon domain mapping of (a) test gather 1 and (b) test gather 2. Mute lines are shown as dark lines. Note sparseness of data mapping, due to Cauchy regularization.

With the amplitude pattern of interface response events described by equation 1, we can produce synthetic models for interface-response amplitude patterns as a function of offset. This pattern alone can be an effective model for the estimation of 1D (in offset) signal PEFs. This is the option that we choose for test gather 1 (signal model shown in Figure 5a, using a constant velocity of 2000 m/s to determine the Fresnel zone size based on a frequency of 400 Hz). Similarly, the pattern model we use for test gather 2 (Figure 6a) was constructed using equation 1 to calculate the amplitude as a function of offset (using a constant velocity of 350 m/s and a frequency of 150 Hz), and using a generalized waveform (the spatially averaged time series of test gather 2) to determine a time signature that adequately mimics the data. Though the waveform of the added events (Ricker wavelet) would have likely been more effective, this approach would be unrealistic in its use of a priori information about the hidden events.

Garambois and Dietrich (2001) show that the time derivative of horizontal geophone data can be very similar to the coseismic noise for the case of compressional waves. The use of geophone data as a pattern model for **N** holds good promise, and it is the option that we use as a noise model for test gather 1 (Figure 5b). Unfortunately, the

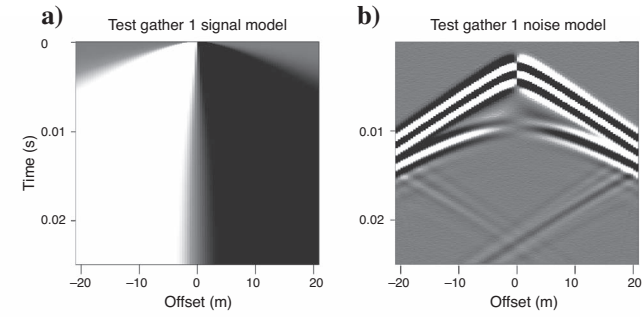

Figure 5. Models for PEF estimation for test gather 1. (a) Signal model, created using equation 1. (b) Noise model, the time derivative of horizontal geophone data, created through the same finite-difference approach as the synthetic seismoelectric data.

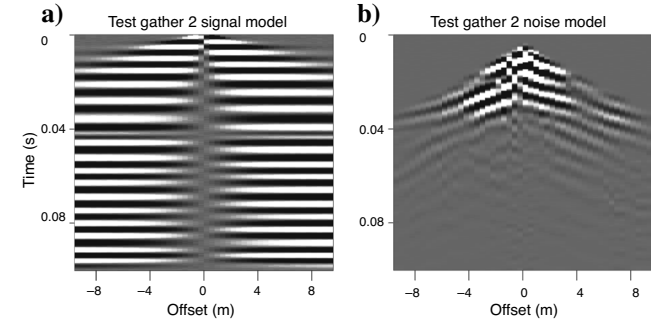

Figure 6. Models for PEF estimation for test gather 2. (a) Signal model, created using equation 1 and a waveform extracted from the gather. (b) Noise model, which is the noise model resulting from Radon filtering, muted to remove all energy above the first coseismic arrivals.

quality of the geophone data collected during our field experimentation is not adequate to provide a good noise model for test gather 2 (likely resulting from the nonflat frequency response of the transformers used between the electrodes and the seismograph and from seismic data irregularity caused by old geophones that no longer fit the manufacturer's specifications). Instead, we mute the parts of the Radon noise estimate that extend above the first coseismic arrivals and use the result as a noise model (Figure 6b).

SIGNAL/NOISE SEPARATION RESULTS

Results from the three signal/noise separation techniques are displayed in Figures 7 (test gather 1) and 8 (test gather 2). The data are gained and scaled the same in each section (a, b, and c) and are the same as the plots of the starting data (Figures 1a and 2a, respectively). The polarity of half the traces is flipped for all plots, such that interface response events show constant polarity on opposite sides of the shotpoint. For test gather 1, the shown Radon result (Figure 7b) is the result of simply muting the noise in the Radon domain, because this result shows more evidence of the previously unseen event IR 3 (shown with the arrows). For test gather 2, the displayed Radon result (Figure 8b) was produced by modeling the noise in the Radon domain and subtracting it from the original data in the *t -x* domain. In all of the results, coseismic noise has been significantly attenuated and little dipping energy remains. For test gather 1 (Figure 7), IR 1, 2, and 4 are plainly visible, and IR 3 is faintly visible, particularly in the Radon and PEF results. For test gather 2, added events A (−30 dB original S/N) and C (−33 dB) are plainly visible in Figure 8b and c, and to a lesser extent in Figure 8a. Event B (−41 dB) is evident, though very weak, in Figure 8c and to a lesser extent in Figure 8b.

The transform methods do not adequately separate the flat central parts of the coseismic hyperbolas from the flat interface response signal. Even when central traces are removed from a gather (Figure 8a), a tiny amount of remaining coseismic energy is flat, and is not entirely removed by *f-k* filtering (a much noisier result is obtained when the near-offset traces are included in the processing). Another disadvantage of the transform-based methods is illustrated by Figure 8a — muting in the *f-k* domain has removed the coseismic energy at the expense of the signal amplitudes. Both comparisons show that the Radon method is preferable to *f-k* filtering, particularly in terms of amplitude preservation.

We find the PEF approach to be the most effective, and its superiority is particularly evident in Figure 7c, where virtually no energy remains above the first interface response event. (Compare to the smeared coseismic energy at ~3 to 4 ms in Figure 7a and b). Figure 7c shows virtually no evidence of this flat near-offset coseismic energy, and also shows much better preservation of the original amplitude patterns of the interface response signal than the *f-k* and Radon results. A remnant of the dipping coseismic energy remains as a speckled checkerboard pattern (related to the edges of the patches used for the nonstationary PEFs) which is not problematic because it would stack out of the gather. In test gather 2 PEF result (Figure 8c), we can see that because the PEFs are "aware" of the amplitude pattern of the interface response events, they can better remove the flat noise events that do not fit this amplitude pattern (e.g., the flat noise events visible at ~0.05 s and below 0.08 s in Figure 8b are weaker or absent in Figure 8c).

Though we have used broad tapers on the edges of mute windows and otherwise been careful that our choice of filter parameters does not result in processing artifacts, some of our results do contain flat arrivals that were not present in the original data. Although not truly artifacts, these arrivals are examples of strong, but nonflat, energy leaking through the signal/noise separation processing. In test gather 1 (Figure 7), the direct and reflected coseismic events arrive simultaneously at ~11 ms and interfere constructively to result in energy that is identified as signal by all three processing methods and appears in the results as flat arrivals at offsets greater than 10 or 15 m. The same is true for the near-offset coseismic arrivals in the test gather 2 between 0.02 and 0.04 s (Figure 8b and c). A solution to this problem is not immediately obvious because we have already chosen our processing parameters to minimize these problems. The flat arrivals below 0.08 s in Figure 8c and d are present in the original data as discussed earlier, so they are not the result of any processing problems. Such noise is best avoided during data acquisition, because it

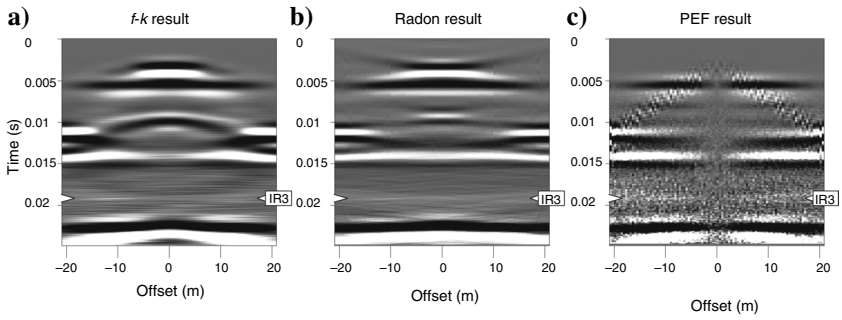

Figure 7. Comparison of signal/noise separation results for test gather 1. All are plotted with gain correction of t^2 and at the same scale as the starting data in Figure 1a. (a) The *f-k* result. (b) Radon result. (c) PEF result. The position of hidden event IR 3 is marked by the arrows on each panel, and this event is faintly visible in all results, particularly in (b) and (c).

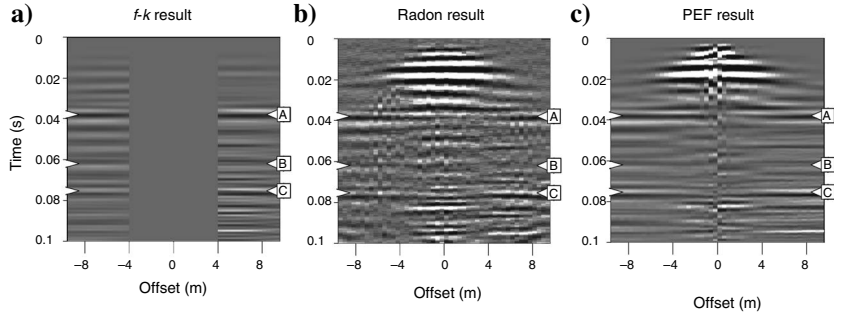

Figure 8. Comparison of signal/noise separation results for test gather 2. All are plotted with gain correction of $t^{1.85}$ and at the same scale as the starting data in Figure 2a. (a) The *f-k* result. (b) Radon result. (c) PEF result. The added events are marked by the three sets of arrows on each panel. Other flat events are discussed in the text.

would be very difficult to separate from simultaneously arriving signal events.

DISCUSSION

As with seismic data, the exact processing flow for a seismoelectric data set must be determined on a case-by-case basis. However, we find the following generalized sequence to be effective:

1) Removal of 60-Hz noise and its harmonics using sinusoidal subtraction (Butler and Russell, 1993), or frequency revision (Butler and Russell, 2003) if sinusoidal subtraction proves insufficient. Both methods provide best results when a signal-free window of the data is available for noise estimation (often pretrigger recording).
2) Minimize background noise and coseismic energy with frequency filtering.
3) Use time-varying gains to adjust amplitude levels as necessary for signal/noise separation.
4) Signal/noise separation using
   a) Linear Radon transform filtering if data quality is good and if gathers have a sufficient number of traces ($\sim$48).
   b) Nonstationary prediction-error filters (PEFs) if computationally feasible and if adequate pattern models can be obtained for PEF estimation.
5) Display processing, such as frequency filtering and gains (AGC or $t^x, x \approx 2$).

As with seismic data processing, it is preferable to use techniques that do not require time-consuming trial-and-error determination of parameters (the PEF and Radon techniques described here may be effective but are costly). Another key requirement is that the signal/noise separation method can not require a priori information about the arrival times of interface response events. Preservation of signal amplitude patterns is an important criterion for evaluating processing methods, because amplitude allows us to properly interpret arrivals and to distinguish them from flat noise. It is evident in Figures 7 and 8 that the PEF method is most successful in this regard (particularly evident for IR 1, 2, and 4 in Figure 7b versus c); unsurprising, given that it is the only method tested that incorporates the interface-response amplitude pattern. The two transform methods do not generally preserve amplitudes as successfully, though the test gather 2 Radon result (event C in Figure 8b) shows that this method can preserve amplitudes when parameters are chosen carefully and a sparseness constraint is included. Although in theory the *f-k* and Radon results should be similar, the Radon result is considerably better in terms of the final signal-to-noise ratio and also the preservation of data amplitudes (Figure 8a as compared to b). This difference between our *f-k* and Radon results is largely a result of our use of the Cauchy regularization, which leads to better focusing of energy in the Radon domain and permits a cleaner separation of the signal from the noise.

CONCLUSIONS

Signal/noise separation is a very important issue in seismoelectric surveying, on a par with the worst cases of groundroll noise in reflection seismic records. Seismoelectric interface response signals are weak and fall off rapidly with distance from the interface (due to the potential field of a dipole, not absorption), so improved signal/noise separation techniques will permit the observation of signals from deeper layers and facilitate confident interpretation of observed signals. We have demonstrated that pattern-based methods are particularly effective for separating the interface response signal from the coseismic fields, successfully isolating signals with an S/N ratio at least as small as –33 dB. These results represent a first step toward development of data processing methods for near-surface seismoelectric surveys, though the results can also be extended to seismoelectric data from exploration depths and to other, similar, data processing cases (e.g., the separation of flat primary arrivals from curved multiple arrivals in the seismic reflection image domain).

In this paper we assume that all subsurface interfaces are horizontal, not a realistic assumption in most settings. It will be necessary to develop the seismoelectric analog to seismic migration for seismoelectric surveying in areas of complex geology. Dipping subsurface layers produce interface-response energy radiating from Fresnel zones that are not directly beneath the shotpoint, necessitating migration to properly arrange seismoelectric energy into CDP-type gathers for stacking. We have focused entirely on signal/noise separation in the shot domain, but transformation to other domains (e.g., seismoelectric CDP domain), and processing within them, will likely be an important issue.

The two principal test data gathers used in our comparisons are both for a "reflection" geometry; that is, a surface survey to image layers at depth. Alternatively, the data in the power line noise comparison were recorded in a "transmission" geometry — the source and receivers are separated and the target is between them. The transmission geometry can provide time-domain separation of signal from noise (the interface response is created and recorded before the coseismic fields are recorded), such that data processing can be accomplished with a simple mute. We have focused on the reflection geometry because it is generally more feasible for data collection. However, the transmission geometry (e.g., crosswell surveying) should also be considered as a possible solution to the problem of seismoelectric signal/noise separation.

We hope that the estimates of processing-method effectiveness provided for the described techniques (in terms of signal/noise ratio in dB) can be used in combination with S/N predicted by numerical modeling to facilitate target selection and to provide a framework within which we can design experiments that have realistic, and known, chances of success. Though admittedly inexact, these estimates establish a basis for assessing whether a given survey target is reasonable. It can be anticipated that as additional data sets are collected and compared with numerical simulations, and as data processing methods are more broadly tested, these estimates will become more exact, which will in turn facilitate the successful application of the seismoelectric method to real geophysical problems.

ACKNOWLEDGMENTS

We are grateful to Steve Pride, Simon Klemperer, and Jerry Harris for valuable guidance in this project. The field data were collected at the Pride Mountain Vineyards in St. Helena, California, thanks to the generous hospitality of Jim and Carolyn Pride, and with the help of Rufus Catchings, Morgan Brown, Mike Beman, Ashley Griffith, Jesse Lomask, and Rob Sanders. Acknowledgment is made to the donors of the American Chemical Society Petroleum Research Fund for support of this research. The work would not be possible without the generosity of the Geological Society of America Foundation, the

American Association of Petroleum Geologists, the Stanford School of Earth Sciences McGee Fund, the Achievement Rewards for College Scientists Foundation, and the sponsors of the Stanford Exploration Project. This paper has been considerably improved by comments from associate editor John Bradford and reviewer Karl Butler, along with two anonymous reviewers.

REFERENCES

Butler, K., A. Kepic, and M. Rosid, 2002, An experimental seismoelectric survey for groundwater exploration in the Australian Outback: 72nd Annual International Meeting, SEG, Expanded Abstracts, 1484–1487.

Butler, K. E., and R. D. Russell, 1993, Subtraction of powerline harmonics from geophysical records: Geophysics, **58**, 898–903.

——–, 2003, Cancellation of multiple harmonic noise series in geophysical records: Geophysics, **68**, 1083–1090.

Claerbout, J., and S. Fomel, 2001, Geophysical estimation by example: Stanford Exploration Project.

Garambois, S., and M. Dietrich, 2001, Seismoelectric wave conversions in porous media: Field measurements and transfer function analysis: Geophysics, **66**, 1417–1430.

——–, 2002, Full waveform numerical simulations of seismoelectromagnetic wave conversions in fluid-saturated stratified porous media: Journal of Geophysical Research, **107**, doi: 10.1029/2001JB000316.

Guitton, A., 2005, Multiple attenuation in complex geology with a pattern-based approach: Geophysics, **70**, no. 4, V97–V107.

Guitton, A., and W. Symes, 2003, Robust inversion of seismic data using the Huber norm: Geophysics, **68**, 1310–1319.

Haines, S., 2004, Seismoelectric imaging of shallow targets: Ph.D. thesis, Stanford University.

Haines, S., A. Guitton, B. Biondi, and S. Pride, 2003, Development experimental methods in electroseismics: 73rd Annual International Meeting, SEG, Expanded Abstracts, 560–563.

Haines, S., and S. Pride, 2006, Seismoelectric numerical modeling on a grid: Geophysics, **71**, no. 6, N57.

Haines, S., S. Pride, S. Klemperer, and B. Biondi, 2004, Development of electroseismic experimental methods: Symposium on the Application of Geophysics to Engineering and Environmental Problems, Environmental and Engineering Geophysical Society, Expanded Abstracts, 1490–1503.

——–, 2007, Seismoelectric imaging of shallow targets: Geophysics, this issue.

Kepic, A., and M. Rosid, 2004, Enhancing the seismoelectric method via a virtual shot gather: 74th Annual International Meeting, SEG, Expanded Abstracts, 1337–1340.

Landau, L., and E. Lifshitz, 1984, Electrodynamics of continuous media, 2nd ed. Pergamon Press Inc.

Pride, S. R., and M. W. Haartsen, 1996, Electroseismic wave properties: Journal of the Acoustical Society of America, **100**, 1301–1315.

Pride, S., and D. Morgan, 1991, Electrokinetic dissipation induced by seismic waves: Geophysics, **56**, 914–925.

Sacchi, M. D., and T. J. Ulrych, 1995, High-resolution velocity gathers and offset space reconstruction: Geophysics, **60**, 1169–1177.

Sava, P., and A. Guitton, 2005, Multiple attenuation in the image space: Geophysics, **70**, no. 1, V10–V20.

Sheriff, R., and L. Geldart, 1995, Exploration seismology, 2nd ed.: Cambridge University Press.

Thompson, A. H., and G. A. Gist, 1993, Geophysical applications of electrokinetic conversion: The Leading Edge, **12**, 1169–1173.

Thorson, J. R., and J. F. Claerbout, 1985, Velocity stack and slant stochastic inversion: Geophysics, **50**, 2727–2741.

Yilmaz, O., 2001, Seismic data analysis, vol. 1: SEG.